Title

The impact of common variants on gene expression in the human brain: from RNA to protein to schizophrenia risk

Authors

Qiuman Liang[1†], Yi Jiang[1,2†], Annie W. Shieh[3], Dan Zhou[4,5], Rui Chen[5], Feiran Wang[1], Meng Xu[1], Mingming Niu[6], Xusheng Wang[7], Dalila Pinto[8,9,10,11], Yue Wang[12], Lijun Cheng[13], Ramu Vadukapuram[14], Chunling Zhang[15], Kay Grennan[16], Gina Giase[17], The PsychENCODE Consortium[‡], Kevin P White[18], Junmin Peng[6], Bingshan Li[5], Chunyu Liu[1,16*], Chao Chen[1,19*], Sidney H. Wang[3*]

Affiliations

1 MOE Key Laboratory of Rare Pediatric Diseases & Hunan Key Laboratory of Medical Genetics, School of Life Sciences, and Department of Psychiatry, The Second Xiangya Hospital, Central South University, Changsha, Hunan 410000, China.

2 Department of Epidemiology and Biostatistics, Ministry of Education Key Laboratory of Environment and Health, School of Public Health, Tongji Medical College, Huazhong University of Science and Technology, Wuhan, Hubei 430000, China.

19 3 Center for Human Genetics, The Brown foundation Institute of Molecular Medicine,
20 The University of Texas Health Science Center at Houston, Houston, TX 77030, USA.

21 4 School of Public Health and the Second Affiliated Hospital, Zhejiang University School
22 of Medicine, Hangzhou, Zhejiang 310058, China.

23 5 Department of Molecular Physiology and Biophysics, Vanderbilt Genetics Institute,
24 Vanderbilt University, Nashville, TN 37232, USA.

25 6 Department of Structural Biology, Department of Developmental Neurobiology, Center
26 for Proteomics and Metabolomics, St. Jude Children's Research Hospital, Memphis, TN 38105,
27 USA.

28 7 Department of Genetics, Genomics, and Informatics, University of Tennessee Health
29 Science Center, Memphis, TN 38163, USA.

30 8 Department of Psychiatry, and Seaver Autism Center for Research and Treatment, Icahn
31 School of Medicine at Mount Sinai, New York, NY 10029, USA.

32 9 Department of Genetics and Genomic Sciences, and Icahn Institute for Data Science and
33 Genomic Technology, Icahn School of Medicine at Mount Sinai, New York, NY 10029, USA.

34 10 The Mindich Child Health and Development Institute, Icahn School of Medicine at
35 Mount Sinai, New York, NY 10029, USA.

36 11 Friedman Brain Institute, Icahn School of Medicine at Mount Sinai, New York, NY
37 10029, USA.

12 Department of Electrical and Computer Engineering, Virginia Polytechnic Institute and State University, Arlington, VA 22203, USA.

13 Institute for Genomics and Systems Biology, University of Chicago, Chicago, IL 60637, USA.

14 Department of Psychiatry, The University of Texas Rio Grande Valley, Harlingen, TX 78550, USA.

15 Department of Neuroscience and Physiology, SUNY Upstate Medical University, Syracuse, NY 13210, USA.

16 Department of Psychiatry, SUNY Upstate Medical University, Syracuse, NY 13210, USA.

17 The Feinberg School of Medicine, Northwestern University, Chicago, IL 60611, USA.

18 Department of Biochemistry, Yong Loo Lin School of Medicine, National University of Singapore, Singapore 117596, Singapore.

19 Furong Laboratory, Changsha, Hunan 410000, China.

† These authors contributed equally to this work.

‡ PsychENCODE Consortium authors and affiliations are listed in the supplementary materials.

* Corresponding author email: Hsi.Ming.S.Wang@uth.tmc.edu (S. H. Wang), chenchao@sklmg.edu.cn (C. Chen), LiuCh@upstate.edu (C. Liu)

Abstract

Background

The impact of genetic variants on gene expression has been intensely studied at the transcription level, yielding invaluable insights into the association between genes and the risk of complex disorders, such as schizophrenia (SCZ). However, the downstream impact of these variants and the molecular mechanisms connecting transcription variation to disease risk are not well understood.

Results

We quantitated ribosome occupancy in prefrontal cortex samples of the BrainGVEX cohort. Together with transcriptomics and proteomics data from the same cohort, we performed cis-Quantitative Trait Locus (QTL) mapping and identified, at 10% false discovery rate, 3,253 expression QTLs (eQTLs), 1,344 ribosome occupancy QTLs (rQTLs), and 657 protein QTLs (pQTLs) out of 7,458 genes from 185 samples. Of the eQTLs identified, only 34% have their effects propagated to the protein level. Further analysis on the effect size of prefrontal cortex eQTLs identified from an independent dataset clearly replicated the post-transcriptional attenuation of eQTL effects. We identified omics-specific QTLs and investigated their potential in driving disease risks. Using both a variant-based approach and a gene-based approach, we identified genes containing expression-specific QTLs (esQTLs), ribosome-occupancy-specific QTLs (rsQTLs), and protein-specific QTLs (psQTLs). Among the variant-based omics-specific QTL, 38 showed strong colocalization with brain associated disorder GWAS signals, 29 of them are esQTLs. From the gene-based approach, we found 11 brain associated disorder risk genes that are driven predominantly by omics-specific QTL, all of them are driven by variants impacting transcriptional regulation. To take a complementary approach to further investigate the functional relevance of genes driven predominantly by attenuated eQTL signals, we identified SCZ risk

genes using each omics independently and then investigated the omics-specificity of the driver regulatory process for each risk gene. Using S-PrediXcan we identified 74 SCZ risk genes across the three omics, 30% of which were novel, and 67% of these risk genes were confirmed to be causal in a MR-Egger test. Notably, 52 out of the 74 risk genes were identified using eQTL data and 68% of these SCZ-risk-gene-driving eQTLs show little to no evidence of driving corresponding variations at the protein level.

Conclusion

The effect of eQTLs on gene expression in the prefrontal cortex is commonly attenuated post-transcriptionally. Many of the attenuated eQTLs still correlate with GWAS signals of brain associated complex disorders, indicating the possibility that these eQTL variants drive disease risk through mechanisms other than regulating protein expression level. Further investigation is needed to elucidate the mechanistic link between attenuated eQTLs and brain associated complex disorders.

Introduction

Complex diseases such as neuropsychiatric disorders are multi-factorial with genetic components (*1*, *2*). Large scale Genome-Wide Association Studies (GWAS) have uncovered thousands of disease associated loci, signaling a promising era ahead for causal variant identification (*3*). However, efforts in fine mapping these disease risk loci often narrowed down the underlying causal signals to non-coding regions of the genome (*4–6*). Regulatory variants in such non-coding regions are therefore the prime candidates for driving the genetic risk of disease etiology. Consequently, integrating gene expression information to pinpoint causal variants or to identify risk genes has become a staple of genetic studies of complex diseases (*7*), with multiple consortia

105 efforts facilitating large scale gene expression profiling and regulatory element mapping (*8–10*).
106 Many powerful methods, such as *coloc*, PrediXcan, SMR/HEIDI, to name a few, have also been
107 developed to leverage gene expression information for fine mapping GWAS signals or for
108 identifying underlying risk genes (*11–13*).

109 Brain associated complex disorders, such as neuropsychiatric disorders, are a group of complex
110 diseases that can be highly heritable (*14*). For example, schizophrenia (SCZ), a psychiatric
111 disorder affecting ~1% of the world-wide population (*15*), has a heritability estimate ranged
112 between 60% to 80%, indicating a strong genetic component (*16*, *17*). Accordingly, recent SCZ
113 GWAS study reported by Trubetskoy et al. identified 287 significant risk loci and prioritized 120
114 risk genes using functional genomics (*18*). The use of RNA-Seq data from the brain was
115 instrumental for risk gene prioritization by Trubetskoy et al., however, information from
116 downstream gene regulation processes, such as translation rate and protein abundance, was either
117 not utilized or unavailable.

118 Measuring transcriptional changes as a proxy for gene activity has a long history in molecular
119 biology (*19*). In the context of human genetics, buffering of downstream effects of genetic
120 variants impacting gene expression (i.e. an eQTL) has been shown to be prevalent (*20*). In
121 addition, QTLs specific to protein level have also been reported (*20-22*). Together, these
122 observations indicated the importance and potential benefits of including downstream omics
123 types, such as proteomics data, as information sources for fine mapping disease regulatory
124 variants. Indeed, recent studies using multi-omics approaches have demonstrated increased power
125 for risk gene identification among other benefits (*23*, *24*). Of note, our recent work on genetic
126 variants associated with protein expression level in prefrontal cortex of the human brain indicated
127 the contribution from non-synonymous coding variants to the changes in protein expression level,

128 and the utility of these protein QTL variants in prioritizing GWAS risk genes for psychiatric
129 disorders (*22*).

130 Another potential benefit of taking a multi-omics approach for identifying disease risk genes rests
131 in the potential to dissect the fine details of regulatory mechanisms driving the disease-genotype
132 association. Having relevant datasets to illuminate the origin and propagation of genetic impact
133 could potentially arrive at a driver regulatory process from a risk variant to a risk gene. Ribo-seq
134 is a technology that fills in the gap between transcript and protein expression. By adapting RNA-
135 Seq to a ribosome footprinting method, ribo-seq provides transcriptome-wide quantification of
136 ribosome occupancy (*25*, *26*), which can serve as a proxy for the amount of active translation
137 synthesizing proteins from each mRNA transcript. When analyzed in conjunction with RNA-Seq
138 and quantitative proteomics data, ribo-seq enables identification of translational and post-
139 translational regulatory events (*20, 27*), both major steps defining the Central Dogma of
140 molecular biology.

141 As a part of the consortium efforts to improve our understanding of the genetic basis of
142 neuropsychiatric disorders (*28*), we generated multiple data modalities that included SNP
143 genotyping, RNA-Seq, ribo-seq, and proteomics of postmortem cortical tissue samples of the
144 BrainGVEX cohort, which altogether covered the major steps of the Central Dogma. In
145 conjunction with the quantitative proteomics and transcriptome profiling results that we
146 previously published (*22*, *29*), here we integrated ribo-seq data as our operational definition for
147 protein synthesis, based on the ribosome occupancy level across the transcriptome, to advance our
148 multi-omics investigation. Our results reveal regulatory properties of common variants and their
149 utility in identifying the regulatory processes in the human brain driving disease risk for brain-
150 associated complex disorders. It offers an opportunity to dissect and appreciate the regulatory

151 information flow in the biological processes from a population perspective. Additional "rules"
152 including an effect attenuation process is recognized.

153

154 **Results**

155 *Measuring transcriptome-wide ribosome occupancy level in prefrontal cortex of adult human*
156 *brain to quantify the level of protein synthesis*

157 To investigate regulatory impact of genetic variants on protein synthesis in the prefrontal cortex
158 of the human brain, we performed ribosome profiling on 211 prefrontal cortex samples from the
159 BrainGVEX collection. In total we collected ~62 billion ribosome profiling reads. Consistent with
160 the expected ribosome footprint size, we found the average insert size of our ribo-seq libraries to
161 range between 27.4 and 29.5 nucleotides. Similar to prior published studies (*30*), we found on
162 average 74 % of unwanted reads from ribosomal RNA, tRNA, and snoRNA, which contributed
163 no information to the translation of protein coding genes. After removing these unwanted reads,
164 we obtained an average of 30.3 million uniquely mapped informative reads per sample (inter-
165 quartile range: 20.5 ~ 37.6 million reads) (Fig. S1A). Focusing on the informative reads, we
166 found the majority (i.e. 84%) of our ribo-seq reads mapped to coding sequence (CDS) exons (Fig.
167 S1B). Moreover, when visualized in aggregate across annotated coding genes, we found our ribo-
168 seq data to show strong sub-codon periodicity at the expected positions (Fig. S1C). High
169 proportion of CDS exon reads and strong sub-codon periodicity indicates the enrichment of
170 footprints from ribosomes actively engaged in translating mature mRNA and reflects the quality
171 of the dataset.

172 *Multi-omics cis-QTL mapping identified candidate regulatory variants and revealed translational*
173 *and post-translational attenuation of eQTL effects*

174 To identify variants associated with inter-individual expression differences, we perform cis-QTL
175 mapping for each omics type independently. From the full dataset we filtered out low coverage
176 genes and removed potentially low quality samples (see details in Data processing section in
177 Materials and Methods) to reach a mapping dataset of 416 RNA-Seq samples, 195 ribo-seq
178 samples, 268 proteomics samples, and the corresponding genotype data. Using the mapping
179 dataset, we identified 12,411 eQTLs (out of 16,540 genes we deem sufficiently quantitated),
180 2,849 rQTLs (out of 14,572 genes), and 1,036 pQTLs (out of 8,013 genes) at FDR < 0.1. Overall,
181 we observed similar genomic feature enrichment patterns of QTL variants across the three omics
182 types (Fig. S2). On the other hand, when focusing on coding variants, we found pQTL to have the
183 largest proportion of coding variants (pQTL: 11.5% vs. eQTL: 3.4% vs. rQTL: 5.1%). Among the
184 coding variants, we found 82.4% were missense variants for pQTL comparing to 56.2% for rQTL
185 and 46.4% for eQTL (Fig. 2A). Of note, we found three start loss variants (i.e. nonsynonymous
186 substitutions in start codons) in rQTL, which was not found in eQTL.

187 Intriguingly, we found drastic differences between omics types in the numbers of QTLs mapped
188 with far fewer rQTLs and pQTLs identified, suggesting reduction of genetic effect along the path
189 of Central Dogma. However, the differences in the number of genes tested between omics types
190 and the differences in sample size complicate the interpretation. To better compare the effects of
191 genetic regulation across data modalities, we identified 185 samples with 7,458 genes that were
192 sufficiently quantitated across all three omics types (Fig. S3). Using this subset of data, we found
193 3,253 eQTLs, 1,344 rQTLs, and 657 pQTLs at FDR < 0.1 (Fig. 1A, Fig. S4, Table S1, S2, S3).
194 Consistently fewer significant QTLs were identified as we moved downstream the Central Dogma
195 of molecular biology.

196 A challenge in comparing between the numbers of QTLs identified from each omics type rests in
197 the fact that not all true effects were identified. While the majority of the QTLs identified here
198 were replicated in independent datasets (Table S4, S5; Fig. S5), which provides an experimental
199 support for our discoveries, the level of false negative rates is less clear. Tests replicating QTLs
200 identified from one omics type in the other omics types can better capture the proportion of
201 genetic effects shared between QTL types. We performed replication tests using $\pi 1$ estimates
202 from the qvalue method (*31*). Overall, we found high proportion of QTLs replicated in other
203 omics types (Fig. 1B). However, when considering the replication rates with the direction of
204 genetic information flow, we found asymmetric replication rates, with the downstream omics
205 types to replicate less than the upstream omics types. More specifically, we found 84.7% of the
206 rQTLs were replicated at the transcript level, but only 60.2% of the eQTLs were replicated at the
207 ribosome occupancy level. Moreover, while 75.9% of the pQTLs were replicated at the transcript
208 level, only 34.0% of the eQTLs were replicated at the protein level (Fig. 1B). A similar
209 asymmetry in proportion replicated between upstream and downstream omics types was observed
210 when using a direction-aware cutoff-based approach across a wide range of significance cutoffs
211 (Fig. S6). The lower percentages of eQTLs and rQTLs replicated at the protein level indicate
212 potential effect attenuation (i.e. either the inter-individual variation in gene expression becoming
213 smaller and therefore harder to detect or a lack of such effect in the downstream omics types).
214 Such effect attenuation at the protein level has been previously reported in lymphoblastoid cell
215 lines (LCLs) (*20*). Our brain data revealed an additional layer of complexity, where effect
216 attenuation was also observed at the level of mRNA translation.

217 While our replication tests revealed a trend of effect attenuation for eQTL variants in the
218 downstream phenotypes (Fig. 1B), these same observations could alternatively be explained by
219 differences in statistical power between technologies. An independent piece of evidence that is
220 not sensitive to measurement precision is needed to reach a solid conclusion. Fold change

221 estimates from less precise measurements are noisier but not biased. In other words, by directly
222 comparing QTL impact on expression level change across omics types we could gain a direct
223 view of effect size attenuation. One issue that remains is that using eQTLs identified from our
224 dataset could bias the results by artificially inflating the variant pool with large eQTL effect sizes,
225 which might arise simply from applying the QTL mapping procedure to the same dataset (i.e., a
226 technical ascertainment bias). Using eQTLs independently identified from prefrontal cortex
227 samples by the CommonMind Consortium (CMC) (*32*), we avoid the ascertainment bias and can
228 therefore compare the effects size of eQTL variants between the three omics types using our
229 dataset. A similar approach was successfully implemented to address this power issue in previous
230 work in LCLs (*20*). Using 5,915 CMC eQTLs that were also quantitated in our dataset, we found
231 the eQTL effects on the transcript expression level to be significantly larger than their effects on
232 ribosome occupancy level (per allele $\log_2$ fold differences: mRNA 0.2433 [95% CI=
233 0.2381~0.2486] vs. ribosome occupancy 0.1836 [95% CI= 0.1794~0.1878]), which were in turn
234 significantly larger than their effects on protein level (per allele $\log_2$ fold differences: 0.1486
235 [95% CI= 0.1451~0.1522]) (Fig. 1C, t-test $P < 2.2e^{-16}$ for all pairwise comparisons). Moreover,
236 for these CMC eQTLs, we found translational regulation to account for more effect size reduction
237 than post-translational regulation (Fig. 1C). By focusing on the effect sizes of independently
238 identified eQTLs, our results strongly support the presence of downstream mechanisms
239 attenuating eQTL effects both at the ribosome occupancy level (translationally) and at the protein
240 level (post-translationally). A complementary analysis looking at the effect size of pQTL variants
241 identified from an independent study (*33*) further supported our conclusion. We found, in our
242 dataset, larger effect size at transcript level when comparing to the fold change at protein level for
243 these independently identified pQTL SNPs (Fig. S7). We noticed that for these independently
244 identified pQTL SNPs, the eQTL effect attenuation appears to be predominantly translationally
245 regulated (Fig. S7B; mRNA vs. ribosome occupancy t-test $P = 6.6e^{-15}$ and ribosome occupancy

246 vs. protein t-test P = 0.4). Similar results were observed across a wide range of significance levels
247 used to define pQTL (Fig. S7).

248 In contrast to prior studies in LCL (*20*), we found clear translational attenuation of eQTL effects
249 in prefrontal cortex. To further investigate this apparent discrepancy, we cross referenced the
250 genes associated with eQTL identified in prefrontal cortex samples to those identified in LCL. We
251 found rather limited overlaps: of the 3,253 eQTL associated genes identified in our brain data
252 only 598 (i.e. ~18%) were found associated with a significant eQTL in LCL (Fig. S8A),
253 indicating the possibility that the between study differences in eQTL discoveries could play a role
254 in the observed differences in translational attenuation of eQTL effects. Indeed, when inspecting
255 the downstream effect of LCL specific eQTL versus a set of effect size matched brain specific
256 eQTL in our brain dataset we found no attenuation of eQTL effect at the ribosome occupancy
257 level among LCL specific eQTL while translational attenuation of eQTL effect remains
258 significant among brain specific eQTLs (Fig. S8B). On the other hand, the shared eQTL found
259 between the two studies showed the expected translational attenuation of eQTL effects in the
260 brain dataset (Fig. S8C), again supporting the notion that the distinct groups of eQTL analyzed
261 between the two studies drive the observed discrepancy.

262 *Identifying omics specific QTLs and their signal colocalization with brain disorder GWAS*

263 The prevalent effect size reduction of eQTLs raised the question of the relevance of these genetic
264 regulation at the organismal level. Because most cellular tasks are executed by proteins, the
265 genetic regulatory effects not reaching the protein level are, presumably, less likely to have an
266 impact on organismal traits. More specifically, we seek the biological relevance of expression
267 specific and ribosome occupancy level specific QTLs (i.e., esQTL and rsQTL). To answer this
268 question, we first set out to investigate the relevance of different QTL types in brain associated

269 complex traits such as neuropsychiatric and neurodevelopmental disorders. By applying mediated
270 expression score regression (MESC) (*34*) to summary statistics from GWAS of four different
271 complex brain disorders and our three types of molecular QTL summary statistics we estimated
272 for each disorder the proportion of heritability mediated by each of our molecular QTL types
273 (Table S6 and Fig. S9). We noticed that for schizophrenia (SCZ), bipolar disorder (BD), and
274 autism spectrum disorder (ASD), eQTL mediated the most heritability, followed by rQTL, which
275 is then followed by pQTL. For example, using the Trubetskoy et al. SCZ GWAS (*18*), we found
276 our eQTLs to mediate 7.09%, rQTLs to mediate 4.06%, and pQTLs to mediate 2.17% of SCZ
277 heritability (Table S6). On the other hand, for major depressive disorder (MDD) all three QTL
278 types mediated similar proportion of heritability (~2.5%).

279 After establishing the relevance for each of the three QTL types in brain associated disorders, we
280 next sought to identify omics-specific QTLs, in order to further evaluate their relevance in driving
281 disease risk. For example, we aim to identify expression specific QTLs (i.e. genetic variants that
282 impact transcript level of the linked genes but not the downstream ribosome occupancy level nor
283 protein level) that colocalize with GWAS signals of brain associated disorders. To identify omics-
284 specific QTLs we took a multiple regression approach by first removing effects of the two other
285 omics-types and then test for genotype association with the residual. To further reduce the number
286 of false positives, for each potential omics-specific QTL identified at 10% FDR we further test
287 genotype association with the other two omics-types and remove any variant that has nominally
288 significant association. We identified 1,553 loci/genes with expression specific QTL (esQTL),
289 155 genes with ribosome occupancy specific QTL (rsQTL), and 161 genes with protein specific
290 QTL (psQTL) (Fig. S10). Similar to standard QTLs we found enrichment of esQTL and psQTL in
291 genomic features such as the exons and the 3'UTRs (Fig. S2). In addition, we found even higher
292 proportion of coding variants and missense variants among psQTLs comparing to the enrichment
293 of these categories reported above for pQTL (Fig. 2A). Of note, we found a clear downward shift

294 in 5'UTR enrichment from pQTL to psQTL (odds ratio 2.51 vs. 1.52, $P < 5e^{-6}$). Similar decrease
295 in 5'UTR variant enrichment was also observed among the other two pairs of standard and omics-
296 specific QTL (i.e., eQTL vs. esQTL and rQTL vs. rsQTL) indicating the possibility that QTL
297 variants in 5'UTR are more likely to be shared across omics types, presumably because they
298 impact protein expression level via transcript level and/or ribosome occupancy level.

299 To identify genes with omics-specific QTL effects driving disease risk, we perform, for each gene
300 containing omics-specific QTL signal, *coloc* analyses with default prior (*11*) between the nominal
301 p value from *cis*-QTL mapping and each brain associated disorder GWAS. We performed
302 separate analysis using either the nominal p value from the omics-specific *cis*-QTL mapping or
303 the standard *cis*-QTL mapping. At a colocalization posterior probability cutoff of 70% we
304 identified risk genes for each omics-type by brain disorder combination for both approaches
305 (Table S7). We found the most risk genes from esQTL loci, with 14 genes showing signal
306 colocalization between SCZ GWAS signals and either standard or omics-specific eQTL signals,
307 and 14 genes for BD, while the remaining combinations resulted in single digit colocalizations
308 (Table S7). For the majority of the risk genes, we observed consistent results between the two
309 approaches (Table S7). On the other hand, we found a few risk genes that have GWAS
310 colocalization with only standard QTL signals, indicating the possibility of GWAS signals
311 colocalizing with QTL signals that were shared with, and therefore regressed out by, other omics
312 types at these loci. In other words, some of these omics-specific QTL were identified from loci
313 containing shared QTL signals that colocalized with GWAS signal.

314 Because regulation of a gene is often modulated by multiple genetic variants, to evaluate the
315 consequence of overall *cis*-QTL impact on gene expression, we use PrediXcan to estimate
316 aggregate genetic regulatory effects for each gene. To identify genes that have omics-specific
317 QTL effects, for each omics type we built PrediXcan models using normalized quantifications

318 with and without regressing out signals from the other omics types. A significant PrediXcan
319 model fit on residuals indicates the potential presence of omics-specific QTL signals (i.e., QTL
320 signals remained after regression). Using a high PrediXcan model fit R^2 cutoff of 0.1 we
321 identified 1,098 candidate genes containing omics-specific QTL signals. To further identify genes
322 with predominantly omics-specific QTL effects we then remove, from the candidate gene list,
323 genes that have either shared QTL effects or additional QTL effects from other omics types by
324 filtering out genes with significant PrediXcan model built from any of the two other omics-types.
325 Using this approach we identified 382 esQTL genes, 36 rsQTL genes, and 51 psQTL genes that
326 have predominantly omics-specific QTL effect. Consistently, these predominantly omics-specific
327 QTL effect genes identified using the PrediXcan gene-based approach are enriched of omics-
328 specific QTL variants identified from the SNP based multiple regression approach (Fig. S11).
329 Colocalization with brain-associated complex disorder GWAS identified 11 risk genes with
330 predominantly omics-specific QTL effects (Table S8). We found most signal colocalization with
331 SCZ, which resulted in 7 SCZ risk genes with predominantly esQTL effects (Fig. 2B).

332 For the remaining 629 candidate genes that potentially contain both omics-specific and shared
333 QTL signals or contain independent omics-specific signals from multiple omics types (i.e. the
334 candidate omics-specific QTL effect genes filtered out from the above step), we use SuSiE to
335 identify independent QTL signals from each omics for each gene (i.e. SuSiE 95% confidence
336 sets). By separating out independent signals form the same gene using SuSiE we can then operate
337 on the confidence set level to identify additional omics-specific QTL signals that colocalize with
338 complex disorder GWAS. We identified a total of 829 confidence sets from 594 candidate genes
339 (Fig. S12). For each confidence set, we perform QTL signal colocalization between omics-types
340 using *coloc*. We found 404 confidence sets to contain QTL signals that are shared with at least
341 one other omics types (i.e. PPH4 > 0.7) while 96 contain QTL signals that are shared across all
342 three omics types (Table S9 full table). Of note, of the 594 candidate genes we found 170 genes to

343 have at least two confidence sets. Among these genes with multiple confidence sets we found
344 examples of separate omics-specific QTL signals from different omics types (Fig. 2C) and
345 example genes that contain both omics-specific and -shared QTL signals (Fig. 2D).

346 To further investigate the relevance of these QTL confidence sets in brain-associated disorders we
347 search for colocalization with brain-associated disorder GWAS signals. Of the 829 confidence
348 sets we found 25 (from 25 genes) to have signal colocalization with at least one of the four brain-
349 associated complex disorders tested. Of these 25 GWAS colocalization signals 13 have QTL
350 signals shared between at least two omics types. Upon visually inspecting the nominal p values
351 from QTL mapping and brain associated disorder GWAS signals at these risk loci we found a few
352 genes with apparently differential colocalization results between confidence sets. For example, we
353 found *RCBTB1* to have two eQTL confidence sets while only one of the two confidence sets
354 contain eQTL signals colocalizing with SCZ GWAS (PPH4 = 0.8). Interestingly, the GWAS
355 colocalizing eQTL for the *RCBTB1* locus appears to be omics specific while the other confidence
356 set appears to contain a QTL signal that is shared between transcript expression and ribosome
357 occupancy (PPH4 = 0.7) (Fig. 2E).

358 *Functional genomics identification of Schizophrenia risk genes*

359 To further investigate the relevance of attenuated eQTLs in brain disease risk, we next took a
360 complementary approach by first identifying risk genes from each omics type separately and then
361 investigating the relevant regulatory processes driving disease risks. Given that we observed the
362 highest number of risk genes for SCZ from our omics-specific QTL analyses, here we focused on
363 SCZ. We applied S-PrediXcan (*35*) on the Trubetskoy et al SCZ GWAS data and our subset of
364 multi-omics data. At 5% family-wise error rate, we found 52, 29, and 16 SCZ risk genes,
365 respectively from RNA-Seq, ribo-seq, and proteomics data (Fig. 3A, Fig. S13). Consistently,

366 when comparing the corresponding GWAS-QTL *coloc* results between genes that passed and
367 genes that failed the S-PrediXcan tests, we found S-PrediXcan risk genes to have higher
368 colocalization posterior probability (Fig. S14). Among S-PrediXcan risk genes only four genes,
369 *NEK4*, *KHK*, *CNNM2* and *DARS2* were consistently identified as SCZ risk genes from all three
370 omics types (Fig. 3B). The majority (74.3%) of the risk genes were identified only from one of
371 the three omics types. This limited sharing in risk gene identification between omics types is
372 consistently observed across multiple significance levels and is in clear contrast to the amount of
373 signal sharing found between QTL types (Fig. 1B; Fig. S15; Table S11, S12, S13).

374 Among the 74 risk genes we identified using S-PrediXcan (i.e. the union of the risk genes
375 identified from each of the three omics types), 44 have previously been reported in GWAS studies
376 as either the mapped genes or as one of the nearby genes under the GWAS peak (Table S14) (*18*,
377 *23, 29*, *36–39*). Of these previously reported genes, 27 matched the mapped genes while the
378 remaining 17 nominated an alternative candidate gene for each GWAS locus (Note that for some
379 of these 17 loci, the original GWAS signals were mapped to an intergenic region). Comparing our
380 results to other published multi-omics SCZ risk gene identification studies, we found 15 matched
381 to the risk genes identified by Giambartolomei et al., which used RNA-Seq and DNA methylation
382 data from prefrontal cortex of the human brain (*23*), and 12 matched to the 120 prioritized SCZ
383 risk genes from Trubetskoy et al., which used colocalization with eQTL and Hi-C data (*18*).
384 When comparing our results to other published TWAS SCZ risk gene identification studies, we
385 found 19 matched to the risk genes identified by Gandal et al. (*29*), and 21 matched to the risk
386 genes identified by Gusev et al. (*39*) (See Supplemental Table S14 for an extended list of risk
387 gene comparisons to prior TWAS studies). On the other hand, for 22 of our 74 risk genes (30%),
388 we found no match to the known risk gene list (Table S14, bottom rows), which we compiled
389 based on previous GWAS, TWAS, and other functional genomics risk gene identification studies
390 (*18*, *23*, *29*, *36–39*). These "no match" novel risk genes have relatively weak SCZ GWAS signals

391 and are therefore challenging to identify without the additional information provided by our
392 multi-omics QTL dataset. For example, we found strong colocalization between a modest SCZ
393 GWAS signal at *2p23.3* and all three types of molecular QTLs of the gene *KHK* (Fig. 3D).
394 Intriguingly, the *KHK* pQTL is in opposite direction of the *KHK* eQTL and rQTL (Fig. 3C),
395 suggesting a strong post-translational process regulating its protein level in the opposite direction
396 to the transcriptional regulation. *KHK*, Ketohexokinase, plays a pivotal role in fructose
397 metabolism and has been hypothesized to contribute to neuronal glycolysis and the loss of
398 neuronal functions (*40*). In addition to *KHK*, other novel SCZ risk genes have also been reported
399 to participate in neuronal/ cognitive functions: For example, in neuroglial cell lines, silencing of
400 *SNX32* leads to defects in neuronal differentiation (*41*). As another example, *NSF*, N-
401 Ethylmaleimide Sensitive Factor, which encodes a vesicle fusing ATPase, was reported as a
402 causal factor in intelligence traits (*42*).

403 *Analyses of multi-omics dataset reveal regulatory mechanisms of schizophrenia risk genes*

404 While PrediXcan is a powerful tool for GWAS risk gene identification, it does not control for
405 potential horizontal pleiotropy (*43*). To this end, we performed two-sample Mendelian
406 Randomization (MR) with Egger regression to replicate the risk genes we identified from using S-
407 PrediXcan. Egger regression includes an intercept term, which can be used to evaluate the level of
408 horizontal pleiotropy (*44*). For each risk gene we first used LD-clumping (*45*) to identify the top
409 QTL SNP from each clump (i.e. a group of linked variants defined by the LD cutoff) to serve as
410 strong genetic instruments (*46*). We then tested for the causal relationship between gene
411 regulation (i.e. QTL signal) and SCZ (i.e. GWAS). We used an operational definition of a causal
412 effect based on the MR test results (see Methods). At 10% FDR, of the 97 gene-by-omics
413 combinations (i.e. a total of 74 risk genes including some discovered from more than one omics
414 type), 67.0% (65/97) passed the MR test. Of those 33.0% that failed the MR test, 37.5% (12 out

415 of 32) failed because of horizontal pleiotropy identified by the Egger intercept test (Table S15). A
416 total of 53 risk genes were replicated in at least one of the three omics types. Note that in order to
417 increase our power, we used a relaxed R^2 cutoff of 0.5 for LD-clumping and adjusted for the
418 linkage between instrument variables in our MR tests using generalized IVW and Egger (*47*).
419 Similar causal effects were observed when using either a stringent R^2 cutoff of 0.01 or using
420 SuSiE (the Sum of Single Effects) (*48*) as an alternative approach to select instrument SNPs (Fig.
421 S16). However, these more stringent criteria on instrument variable independence led to lower
422 power to detect and fewer genes available to test (Table S16). For example, when using SuSiE for
423 selecting instrument variables, only 40 genes were tested because some of the risk genes had no
424 fine mapped QTL SNPs according to SuSiE.

425 A key strength of using a multi-omics QTL approach to identify GWAS risk genes rests in the
426 possibility of further narrowing down the potential regulatory mechanisms. To this end, we
427 further examined the likely causal mechanisms for the 53 replicated SCZ risk genes using one-
428 sample Mendelian Randomization to infer causality between QTL types. We focused our analysis
429 on independently testing for causal effects between neighboring QTL types following the
430 direction of information flow of the Central Dogma (i.e. mRNA -> ribosome occupancy, and
431 ribosome occupancy -> protein). Here we used fine-mapped QTL SNPs identified from the
432 exposure omics types (i.e. the upstream omics types) as instrument variables for one-sample MR
433 analysis. Among the 53 MR-Egger replicated SCZ risk genes, we found 21 genes with significant
434 causal effects both from eQTL to rQTL (i.e. the upstream pathway) and from rQTL to pQTL (i.e.
435 the downstream pathway) (both-passed risk genes; Fig. 4A). Significant causal effects detected
436 from both pathways suggest transcriptionally regulated protein level differences as the potential
437 mechanisms driving these risk genes in SCZ etiology (see an example in Fig. 4B). On the other
438 hand, 25 and 7 replicated risk genes have either significant causal effects only in one of the two

439 pathways (single-passed risk genes; Fig. 4A) or have no significant causal effects (none-passed
440 risk genes; Fig. 4A), respectively.

441 Of note, for 23 of the 25 single-passed risk genes, we found significant causal effects in the
442 upstream pathway (mRNA -> ribosome occupancy). This asymmetry is reminiscent of the eQTL
443 effect attenuation described in the prior sections. A failed test could indicate either a true lack of
444 effect or a lack of statistical power. To take a closer look, we directly assessed the effect size, the
445 noise level, and instrument strength of the one-sample MR test results. When comparing to the 21
446 both-passed risk genes, we found clearly smaller effect sizes for the failed tests of both the 7
447 none-passed risk genes (average 0.577 vs 0.058, t-test $P < 10^{-3}$, Fig. S17A) and the 23 single-
448 passed risk genes (average 0.524 vs 0.116, t-test $P < 10^{-3}$, Fig. S18A). Note that in both cases the
449 inter-quartile range of the estimated causal effects for the failed tests covered zero (Fig. S17A,
450 Fig. S18A). For these same comparison groups, we found no significant differences in instrument
451 strength (Fig. S17C and S18C) and found slightly higher noise level in the failed MR tests (Fig.
452 S17B and S18B). When considered together, these observations (i.e. clearly smaller effect size
453 and slightly elevated noise level for the failed tests) indicate that many of these test results reflect
454 a true lack of causal effect while in some cases weak effects were obscured by noise. In other
455 words, many of these risk genes are likely to be driven by either omics-specific QTLs or
456 attenuated eQTLs. Case in point, we found *SF3B1* to have strong signal colocalization between
457 eQTLs and SCZ GWAS without clear QTL signals in either ribo-seq or proteomics data (Fig.
458 4C).

459

460 **Discussion**

461 Using a panel of postmortem prefrontal cortex samples, we found clear evidence of post-
462 transcriptional attenuation of eQTL effects in the human brain. Many of the differences found in
463 transcriptomes were not present in proteomes. This observation echoes earlier work in HapMap
464 lymphoblastoid cell lines (*20*) and extends the prior conclusion from *in vitro* cell lines to complex
465 human tissues. Importantly, distinct from the earlier work in lymphoblastoid cell lines, which
466 found rQTL to mostly track with eQTL, we found clear attenuation of eQTL effect in ribo-seq
467 data indicating that translational regulatory processes are involved in eQTL effect attenuation in
468 the human brain. Our further investigation on this observation indicated that differences in the set
469 of eQTL (eGENE) identified between the two studies explains the discrepancy. However, it
470 remains to be determined whether the discrepancy observed between the two studies reflects a
471 true difference between the tissue/cell types used in these studies, or effects rooted in differences
472 in sample complexity, or effects from other unknown unaccounted for variations, or simply an
473 incidental finding. Prevalent translational attenuation of variant impact on transcriptional gene
474 expression level has previously been reported in budding yeast (*49*, *50*). However, results from
475 follow up studies (*51*) appear to present an inconsistent picture. Here, using replication tests for
476 individual eQTLs and testing for aggregate effect size of eQTLs independently identified from
477 CMC, we provided strong evidences supporting prevalent translational attenuation of eQTL
478 effects in the human brain. Importantly, by focusing on comparing QTL effects (i.e. between
479 genotype fold change) in aggregate, our analyses are robust to power issues resulted from
480 measurement imprecision (random noise). On the other hand, our conclusions could still be
481 sensitive to potential biases in the dataset, which could result from technical issues that cannot be
482 randomized. For this reason we paid close attention to the impact of sequencing coverage (for
483 sequencing data) and ratio compression (for quantitative mass spectrometry data) on our major
484 conclusion. Of note, our quantitative mass spectrometry study employed an analytical procedure
485 that adjusts for contaminating background signals in order to correct for potential ratio

compression in quantification (*52*). Consistently, among low abundance proteins, which are more susceptible to the influence of ratio compression, we did not find a disproportional decrease in pQTL effect size (Fig. S19C). Similarly, while genes with low expression level are more sensitive to issues related to low sequencing coverage, we found little to no correlation between eQTL/rQTL effect size and expression level (Fig. S19A, S19B). Although ample precautions and multiple distinct approaches were taken to confirm the observed effect size attenuation, it remains possible that unknown, unaccounted for omics-specific features could potentially confound the results. In other words, although operating at the molecular level, our study remained observational. Future work replicating this observation and elucidating molecular mechanisms of post-transcriptional attenuation of eQTL effects are needed to provide a clear understanding of the phenomenon.

Although our study was not designed to answer the key questions regarding the underlying mechanisms of the observed translational and post-translational attenuation of eQTL effect, the high prevalence of the observed eQTL effect attenuation when considered in conjunction with the low prevalence of coding mutations in human population provides some hints. Since a compensatory variant driving translational or post-translational attenuation is expected to be either a coding mutation that impact translation elongation rates or protein turnover rates or a UTR variant that impacts translation initiation rate, the apparent mismatch in incident prevalence indicated that compensatory variants are unlikely to explain the majority of the effect size attenuation and therefore implies a broad-spectrum mechanism that reduce variation at the protein level across genes. Consistently, we observed significant translational and post-translational attenuation of eQTL effect across all PhastCons score strata on top of a clear trend of decreased QTL effect size as the evolution conservation scores increase (Fig. S20). Our current work focuses on the other important follow-up question of whether the attenuated eQTLs are functionally (biologically) relevant. We attempted to address this question by exploring the

511 relevance of attenuated eQTLs in brain associated disorders, such as SCZ, a neuropsychiatric
512 disorder that is highly heritable. We took multiple approaches to identify risk genes that have
513 either omics-specific QTL signals or attenuated eQTLs. In one approach, we used regression
514 based methods to identify omics-specific QTL performing separate analysis either at the SNP
515 level or using PrediXcan to aggregate variant impact at the gene level. In both cases, we found the
516 most number of colocalization between esQTL and complex disorders (i.e. comparing to rsQTL
517 and psQTL). From the gene level analysis we further identified interesting example genes
518 containing multiple QTL signals with varying level of omics-specificity, including an example
519 gene, *RCBTB1.* We found two strong eQTL signals at *RCBTB1*, while one potentially shared and
520 one potentially omics-specific. Only the apparently omics-specific eQTL was found to colocalize
521 with SCZ GWAS. These examples illustrate the complexity of variant impact on gene regulation
522 and disease risks. Regression based approach, however, could produce false positive omics-
523 specific QTL simply from noisy predictors. Although we implemented checks and filters to
524 remove these likely false positives, this caveat is important to keep in mind when interpreting
525 these results.

526 In another approach, we conducted our search by first identified risk genes from all quantitated
527 genes using a TWAS approach, S-PrediXcan method. We then tested for causal regulatory
528 mechanisms driving the risk gene using QTL SNPs as instrumental variable in a one-sample
529 Mendelian Randomization test. Before testing for causal regulatory mechanisms, we first
530 replicated the TWAS risk genes using two-sample Mendelian Randomization with Egger
531 intercept tests. About 30% of the risk genes that we identified here have not previously been
532 reported as SCZ risk genes. The use of our functional genomics dataset is key to the discovery of
533 these novel SCZ risk genes because of their relatively weak GWAS signals (see Fig. 3D for an
534 example). As a reminder, we would like to emphasize the fact that individual risk gene
535 identification is dependent on the choice of significance cutoffs, which is to some extend

536 arbitrary. We used a rather stringent family-wised error rate for risk gene identification in order to
537 reduce the number of false positive results that could mislead researchers interested in molecular
538 biology follow-up studies.

539 To identify causal regulatory mechanisms for each replicated risk gene, we further tested
540 causality between QTL types using one-sample MR. We found 21 risk genes that are likely
541 contributing to SCZ risk through transcriptionally regulated protein level. On the other hand, we
542 also identify 7 genes that show no significant results from MR tests (candidate omics-specific risk
543 genes) and 23 genes that have significant MR test results only from transcription to translation
544 (candidate post-translationally-attenuated risk genes). In essence, attempts to identify omics-
545 specific risk genes (or omics-specific QTLs) are dealing with the challenge of separating true
546 negatives from false negatives. As such, the interpretation of the failed MR tests is challenging.
547 Our subsequent analyses looking at comparing instrument strength, noise level, and effect size
548 between passed and failed MR tests, indicated comparable instrument strength, slightly elevated
549 noise level in the failed tests, and clearly smaller effect size in the failed tests. In other words, it
550 remains possible that some of the failed tests could be reflecting a small effect size obscured by
551 the elevated noise level. In addition to the issues with false negative results, some of the
552 discoveries could be false positives to begin with. Although we have good confidence with our
553 FDR and FWER estimates, given that our test statistics for QTL mapping and risk gene
554 identification are well calibrated (Fig. S4, S13), pleiotropy could introduce positive results from a
555 different underlying cause (i.e. true effects on SCZ risk but false positive risk genes).

556 Power issues, however, do not explain the whole story. As was consistently observed throughout
557 our study, when viewed in aggregate, we see clear effect size differences between omics types,
558 both for QTLs and for causal effects from MR tests. These effect size estimates are not influenced
559 by significance cutoffs and are not biased by power differences. Such general trends are also

560 unlikely to simply be a result of spurious associations or made up entirely of false positives. Our
561 results therefore bring forth an interesting mechanistic question: how do attenuated eQTL variants
562 impact SCZ without changing protein levels? One interesting possibility is that the biologically
563 relevant traits here are protein synthesis rates and protein turnover rates. An association between
564 genotype and protein synthesis rates could manifest in the form of an attenuated eQTL, if the
565 differences in per transcript protein synthesis rate (e.g. differences in ribosome elongation rate or
566 translation initiation rate) appears to offset the differences introduced at the transcript level, which
567 in turn could resulted in a lack of differences in ribosome occupancy level. Similarly a protein
568 turnover QTL could also manifest in the form of a rQTL attenuated at the protein level. In other
569 words, colocalization between an attenuated rQTL and a GWAS signal could actually be
570 reflecting a colocalization of the GWAS signal with a protein turnover QTL. Testing this
571 hypothesis requires a direct measurement of protein turnover rate. We hope by presenting the
572 current results, our findings can inspire future studies on this topic to better understand the
573 regulatory processes from DNA to brain associated disorders.

574

575 **Materials and Methods**

576 **Data sources**

577 The SNP genotypes (*22*), RNA-Seq (*29*), and quantitative mass spectrometry (*22*) data generated
578 for prefrontal cortex tissue samples of the BrainGVEX cohort were downloaded from the
579 PsychENCODE Synapse portal (https://www.synapse.org/#!Synapse:syn5613798) (See Table
580 S18 for a summary on the number of samples in each dataset and their respective overlap with the
581 samples in the genotype data). The BrainGVEX cohort includes 420 Caucasians, 2 Hispanics, 1
582 African American, 3 Asian Americans, and 14 unknown-origin individuals. We also used GWAS

583 summary statistics data of schizophrenia (*18*), bipolar disorder (*53*), autism spectrum disorder
584 (*54*), and major depression disorder (*55*) obtained from the Psychiatric Genomics Consortium.

585 **Ribosome profiling**

586 Ribosome Profiling experiments were performed using Illumina's TrueSeq Ribo Profile
587 (Mammalian) Kit. TrueSeq Ribo Profile (Mammalian) Kit was developed for cell lines. We
588 adapted the protocol to frozen tissue samples with MP Biomedicals™ FastPrep-24™ Classic
589 Bead Beating Grinder and Lysis System. Specifically, 60-80 mg of frozen brain tissue was
590 homogenized in Lysing Matrix D tubes containing 800 µl polysome lysis buffer. The Lysing
591 tubes were placed on the FastPrep-24™ homogenizer set at 4.0 m/s with 20 s increments until no
592 visible chunks of tissue remained. Tissue lysate was incubated on ice for 10 min followed by
593 centrifugation at 20,000g at 4 °C for 10 minutes to pellet cell debris. Clarified lysate was
594 subsequently used for ribo-seq library preparation following TrueSeq Ribo Profile (Mammalian)
595 Kit instructions. Indexed libraries were pooled and then sequenced on an Illumina HiSeq 4000.
596 Note that the experimental protocol for TrueSeq Ribo Profile (Mammalian) Kit that we followed
597 is a modified version of the previous ribo-seq protocol published by Ingolia and colleagues (*26*),
598 and it has the following key modifications: Monosome isolation was performed using Sephacryl
599 S400 spin columns (GE; 27–5140-01) on a tabletop centrifuge instead of ultra-high speed
600 centrifugation in sucrose cushion. Ribosomal RNA depletion was carried out by using Ribo-Zero
601 Magnetic Kits and this step is moved up to right after the monosomal RNA isolation step and
602 before the Ribosome Protected Fragment gel isolation step.

603 **Data processing, gene expression quantification, and normalization**

604 For Genotype data, we obtained Genotype VCF files from PsychENCODE BrainGVEX Synapse
605 portal (https://www.synapse.org/#!Synapse:syn5613798). The VCF file includes data from 420

individuals genotyped using a combination of 3 different platforms. Details on genotyping experiments and data processing can be found in our companion manuscripts (*22, 29*). Briefly, data from whole-genome sequencing (WGS), Human PsychChip platform (a custom version of the Illumina Infinium CoreExome-24 v1.1 BeadChip), and Affymetrix GeneChip Mapping 5.0K Array were separately imputed using Minimac3 with Haplotype Reference Consortium (HRC) reference panel and then merged using PLINK with filters for variant call quality, imputation quality, minor allele frequency, and relatedness. Only variants with genotype (or imputed) $R^2 >$ 0.3, Hardy-Weinberg Equilibrium > 10^{-6} and minor allele frequency (MAF) > 0.01 are kept. The combined and filtered VCF file contains genotype data of 8,108,028 SNPs for 420 individuals. We further evaluated potential effects of additional confounding factors on genotype data (Fig. S21).

For RNA-Seq data, we obtained raw reads in FASTQ format from the PsychENCODE BrainGVEX project (https://www.synapse.org/#!Synapse:syn5613798). We then process the raw reads by removing the adapter sequence using cutadapt (v1.12) code "cutadapt –minimum-length=5 –quality-base=33 -q 30 -a AGATCGGAAGAGCACACGTCTGAACTCCAGTCA -A AGATCGGAAGAGCGTCGTGTAGGGAAAGAGTGT". The cutadapt processed reads were then mapped onto GENCODE Release 19 (GRCh37.p13) genome with transcript annotations from the corresponding version of GTF files using STAR (v2.4.2a). We used RSEM software (v1.2.29) to quantify read counts for each gene (*56*). The cpm function in the R package "limma" was used to calculate the log-transformed counts per million (CPM). We filtered out genes with CPM < 1 in more than 75% of the samples and samples with network connectivity (*57*) z score < -5 (Fig. S22A), which resulted in a total of 17,207 genes from 426 individuals in the quantification table. We then used normalize.quantiles function in the R package "preprocessCore" (*58*) to normalize expression level for each sample. DRAMS software was used to detect and correct mixed-up samples (*59*), which resulted in a final count of 423 individuals.

631 For ribo-seq data, we used cutadapt (v1.12) to remove adapter sequence from raw reads with code
632 "cutadapt -a AGATCGGAAGAGCACACGTCT –quality-base=33 –minimum-length=25 –
633 discard-untrimmed". The processed reads were then mapped against a FASTA file of rRNA,
634 tRNA, and snoRNA sequence downloaded from NCBI using bowtie2 (*60*) to filter out
635 uninformative reads. The filtered reads were mapped to GENCODE Release 19 (GRCh37.p13)
636 genome with corresponding transcript annotation GTF file using STAR (v2.4.2a). The uniquely
637 mapped reads, as defined by the "NH:i:1" flag of the alignment files, were kept for subsequent
638 analysis. We used the featureCounts function in the R package "subreads" (*61*) to calculate gene
639 level read counts for ribosome occupancy. The cpm function in the R package "limma" was used
640 to calculate log-transformed CPM value. We filtered out genes with CPM < 1 in more than 75%
641 of the samples and samples with network connectivity (*57*) z score < -3.5 (Fig. S22B), which
642 resulted in a total of 15,171 genes quantitated from 209 individuals in the quantification table. We
643 then used the normalize.quantiles function in the R package "preprocessCore" (*58*) to normalize
644 ribosome occupancy level for each sample. DRAMS software was used to detect and correct
645 mixed-up samples (*59*), which resulted in a final count of 199 individuals.

646 For quantitative mass spectrometry data, we obtained protein quantification table from the
647 PsychENCODE BrainGVEX Synapse portal (https://www.synapse.org/#!Synapse:syn5613798).
648 This table includes abundance quantification for 11,572 proteins from 268 individuals. The
649 MS/MS raw data were searched against a composite target/decoy human proteome database. The
650 target database contains 83,955 entries, including both canonical proteins and isoforms
651 downloaded from the UniProt database. Since we employed shotgun proteomics, we identified
652 peptides rather than full-length proteins. In cases where a peptide could be mapped to multiple
653 homologous proteins, we followed the rule of parsimony: the peptide was first assigned to the
654 canonical protein. If no canonical form was defined, the peptide was assigned to the protein
655 isoform with the highest uniquely mapped PSM (Peptide-Spectrum Match). For quantification,

656 we summarized all peptides that are mapped to the representative protein. These data processing
657 steps for producing the mass spectrometry quantification table is detailed in Luo et al. (*28*). We
658 further log-transformed protein abundance for each sample. We filtered out genes with log-
659 transformed protein abundance < 1 in more than 75% of the samples and samples with network
660 connectivity (*57*) z score < -6 (Fig. S22C, note that all genes and samples passed the filtering
661 cutoff). We then used the normalize.quantiles function in the R package "preprocessCore" (*58*) to
662 normalize protein level for each sample. DRAMS software was used to detect mixed-up samples
663 (*59*) and found none. We matched protein IDs to gene IDs according to the UCSC database (hg19
664 version), which resulted in protein level quantifications for 8,330 genes. When matching pQTL
665 signals to genes for comparison with eQTLs/rQTLs, we used the pQTL signals associated with
666 the protein isoform that has the highest median abundance.

667 **QTL mapping**

668 *Estimating and adjusting for unwanted factors*

669 We used the R package "PEER" (*62*) to estimate hidden factors for RNA-Seq, ribo-seq, and
670 proteomics data separately. The principle of selecting unwanted hidden factors was to maximize
671 the variance explained with the least number of factors. We identified 30, 29, and 19 hidden
672 factors to remove from RNA-Seq, ribo-seq, and mass spectrometry data, respectively (Fig. S23).
673 For each gene from each omics type, we adjusted the expression level by fitting the selected
674 hidden factors as predictors in a linear model and taking the residuals as the adjusted expression
675 level. The adjusted expression levels were then further centered by mean and scaled by standard
676 deviation.

677 *Genotype association tests*

678 We identified *cis*-region expression QTLs (eQTLs), ribosome occupancy QTLs (rQTLs), and
679 protein QTLs (pQTLs) separately using QTLTools (1.3.1) (*63*). Because each gene can encode
680 several protein isoforms, we selected the protein isoform with the highest median abundance as
681 the representative protein. For each gene, we defined *cis*-region as the region ranging from 1Mb
682 upstream of the 5' end of the gene to 1Mb downstream of the 3' end of the gene (i.e. the length of
683 the gene body plus 2 Mb in size). We tested all common SNPs (MAF > 0.05) within the *cis*-
684 region for each gene. We performed 10,000 permutations to create null distributions to obtain
685 permutation-based p values and further adjusted permutation-based p values used the beta-
686 approximation approach implemented in QTLTools to calculate empirical p values. For each
687 gene, we selected the most significant SNP to represent the QTL signal (i.e. the variant with the
688 smallest empirical p value) and then calculated a genome-wide FDR using the qvalue function of
689 the R package "qvalue".

690 **Annotation and enrichment analyses of QTL variants**

691 We used Ensembl Variant Effect Predictor (VEP) version 105 to annotate QTL SNPs. Each
692 variant was assigned multiple annotations as each variant could map to multiple transcript
693 isoforms of the same gene. We perform three separate analyses with different counting schemes,
694 counting all annotations, counting only most frequent annotations, counting only the annotation
695 with the most severe consequence, to ensure the percentage estimates and conclusions of
696 enrichment are robust.

697 For genomic feature enrichment analysis, we extracted 5' UTRs, exons, introns, 3' UTRs, and
698 intergenic regions from the GENCODE v19 GTF file. The exon regions were extracted directly
699 from entries in the third column of the GTF file (column label: "exon"). Similarly, gene regions
700 were extracted directly from the GTF file. Intron regions were calculated by removing exon

701 regions from gene regions, while intergenic regions were obtained by removing gene regions
702 from the genome. The 5' UTR and 3' UTR coordinates were generated using the
703 fiveUTRsByTranscript() and threeUTRsByTranscript() functions from the R package
704 "GenomicFeatures", respectively. We used bedtools intersect -wa to identify QTL SNPs
705 overlapping each genomic feature. We used Fisher's exact test to evaluate statistical significance
706 of QTL SNP enrichment in each genomic feature. For genic features (e.g., 5' UTRs, exons,
707 introns, 3' UTRs) total genic counts were used as the background; for intergenic features, total
708 cis-region (i.e., mapping window) counts were used as the background.

709 **Estimating mediated heritability of each omics**

710 We used MESC to estimate the proportion of heritability mediated by different omics separately
711 for four different brain-associated disorders (*33*). In the first step, we calculated the overall
712 expression score using the unwanted-factor-adjusted-expression data (see QTL mapping section)
713 as the individual-level gene expression data and the corresponding BrainGVEX genotype data.
714 We used the 1000 genome phase 3 genotype data to calculate LD scores in order to match
715 BrainGVEX genotype data to GWAS genotype data. In the second step, we used the overall
716 expression score calculated in the previous step and GWAS summary statistics to estimate
717 heritability mediated by each omics.

718 **Identifying omics-specific QTL**

719 *SNP-based approach*

720 We used QTLTools to identify omics-specific QTL variants following the same procedure as
721 standard QTL mapping, which is described in the above section, except that the gene expression
722 quantification for the omics-type of interest was adjusted by regressing out signals from the other

723 two omics types. The regression was achieved by including peer adjusted normalized
724 quantification of the other two omics types as covariates in QTLTools. For each gene, we selected
725 the SNP with the most significant genotype-expression association as the candidate omics-
726 specific QTL SNP and used Benjamini-Hochberg procedure to control for false discovery rates.
727 To further remove false positives resulted from ineffective removal of signals from the other two
728 omics types, likely due to poor linear model fit, we removed candidate omics-specific QTLs with
729 nominal significant association (p values < 0.01) with any of the other two omics types.

730 *Gene-based PrediXcan approach*

731 Building prediction models: We used the PrediXcan software (*13*) to separately build gene
732 expression prediction models based on RNA-Seq, ribo-seq, and quantitative mass spectrometry
733 data. We built these models for each gene for each omics type with and without regressing out
734 signals from the other two omics types (i.e. for each gene using data of each omics type we build
735 both a standard model and a residual model). For each model, an Elastic Net algorithm was used
736 for feature selection from SNPs located within the *cis*-region defined for each gene (i.e. gene
737 body +/- 1Mb flanking regions) based on results from a ten-fold cross-validation. Weights were
738 produced for every selected SNP of each gene, which were used in the prediction models. For
739 each model, we calculated the Pearson correlation between the predicted and the observed gene
740 expression (Cross-validation R, R_{cv}), which was considered as a metric for model prediction
741 accuracy. Unless otherwise specified, we consider models with R_{cv}^2 above the PrediXcan default
742 0.01 threshold as models describing genes with significant genetic contribution to expression
743 regulation (*13*). We produced prediction models for the unified set of 7,458 genes from 185
744 samples.

745 Identifying and categorizing genes containing omics-specific genetic effects: We defined genes
746 with significant residual model as candidate genes containing omics-specific QTL signals using a
747 high R_{cv}^2 cutoff of 0.1 in conjunction with a FDR cutoff of 0.05 for the model fit. Of these
748 candidate genes we further classify them by the model fit results from the other omics types. If no
749 significant standard models were built from any of the two other omics-types, we consider the
750 gene as a predominantly omics-specific QTL gene. For example, for a gene with significant
751 residual model built from RNA-Seq data (eQTL signal), if there are no significant standard model
752 built from either ribo-seq nor proteomics data we consider the gene as a predominantly transcript
753 specific QTL gene (esQTL). For candidate genes that have significant model built from any of the
754 other two omics types we consider these candidate genes as potentially harboring multiple QTL
755 signals from different omics types (either omics-specific or shared QTL effects). To separate out
756 independent signals from each gene we used SuSiE to identify 95% confidence sets representing
757 each individual signals. To categorize these independent signals as shared or omics-specific we
758 then perform *coloc* analysis with data from the other omics-types for each confidence set using
759 SNPs in modest LD (squared correlation > 0.01) with the confidence set of interest to ensure
760 sufficient background SNPs and excluding variants that are in linkage (squared correlation > 0.1)
761 with any other confidence sets. For each confidence set we also performed *coloc* analysis with
762 brain-associated disorder GWAS, in order to identify QTL signals driving disease risks among
763 these confidence sets. See the next section for details on signal colocalization analysis using
764 *coloc*.

765 **Colocalization**

766 We used *coloc* (*11*) to detect signal colocalization between brain-associated disorder GWAS and
767 each QTL type at the cis-region of each QTL gene. For each QTL gene, for all common SNPs
768 (MAF > 0.05) within the cis-region, we use QTL effects and GWAS summary statistics of brain

769 associated disorders as input for *coloc* analysis. To estimate QTL effects, we calculated, from a
770 linear model fit using SNP genotype as the predictor for gene quantifications, the predictor
771 regression coefficient and its corresponding square of standard error. We then used the coloc.abf
772 function in the R package "*coloc*" (*11*) to calculate the posterior probability of each hypothesis
773 using the default prior. We use posterior probability of 70% for the colocalization hypothesis (i.e.
774 PPH4) as the cutoff for reporting our colocalization findings.

775 **TWAS identification of SCZ risk genes**

776 We used S-PrediXcan (*34*) to perform gene-level association tests based on the prediction models
777 built using our brain prefrontal cortex multi-omics data, which is described in the "*Gene-based*
778 *PrediXcan approach*" section, and the SCZ GWAS summary statistics data from PGC3 (*18*). The
779 association tests were performed separately for each omics. For protein data, we performed
780 omnibus test to incorporate p values of all protein isoforms together to calculate a single p value
781 for the corresponding gene. The family wise error rates for SCZ risk genes were calculated using
782 Bonferroni correction of nominal p values.

783 **Two-sample Mendelian randomization (MR)**

784 To identify causal relationships between each omics type and SCZ we used MR analysis. Here we
785 used fine mapped QTL SNPs as instruments, gene expression quantification at each omics type as
786 exposure, and SCZ GWAS signal as outcome.

787 More specifically, we took the following steps to test for causal relationship between gene
788 regulation at each omics level and SCZ:

789 Step 1: Here we used two methods for selecting instrument SNPs: an LD clumping approach and
790 a SuSiE approach. For the LD clumping approach, for each gene of each QTL type, we used

791 PLINK with "–clump-kb 1000 –clump-r2 0.5" parameters and a QTL nominal p value cutoff to
792 define instrument SNPs from separate QTL signals. Since our goal is to test as many risk genes as
793 we reasonably can, we used a dynamic (greedy) approach in defining the QTL p value cutoff for
794 instrument SNP selection. We first set a stringent p value cutoff at 10^{-4}, which identified the
795 majority of our instrument SNPs. For genes that don't have at least 3 instrument SNPs identified
796 we incrementally relaxed the p value cutoff first to 10^{-3} and then to 10^{-2}. See Supplemental Table
797 15 for details on the p value cutoffs used for each omics type by risk gene combination.
798 Independent of the above mentioned, we performed a separate MR analysis using LD clumping
799 with $r^2 < 0.01$ to ensure independence between instrument SNPs and a p value cutoff of 0.05. For
800 the SuSiE approach, we used susie_rss() function with default parameters in the R package
801 "SuSiE" (*47*).

802 Step 2: We then used the mr_steiger() function in the R package "TwoSampleMR" to test the
803 causal direction of selected instrument SNPs. For genes failing the Steiger test, we applied the
804 steiger_filtering() function to verify the direction of each instrument SNP and excluded those with
805 incorrect directions, ensuring the explained variance by the instrument SNPs was greater for the
806 exposure than for the outcome.

807 Step 3: For each gene, we used harmonise_data() function in R package "TwoSampleMR" (*64*) to
808 harmonize QTLs of each omics type and SCZ GWAS SNPs to be in the same direction (i.e. effect
809 relative to the same allele).

810 Step 4: We then performed two-sample MR for each gene by omics type combination separately.
811 Two-sample MR analysis was done using the R package "MendelianRandomization" (*65*). We
812 used mr_ivw(data, correl = TRUE) function to conduct generalized IVW and
813 mr_egger(data,correl = TRUE) function to conduct generalized Egger (see next step). Generalized

814 IVW accounts for linkage between instrument SNPs, which enables the MR analysis to use linked
815 instrument SNPs.

816 Step 5: We used the intercept test (i.e. the Egger method) to test for horizontal pleiotropy, and
817 used predictor coefficient and its corresponding p value from IVW to determine the effect size
818 and significance of causal effects for each omics type on SCZ.

819 Step 6: We used Benjamini-Hochberg control procedure to adjust the nominal p values from IVW
820 for multiple testing.

821 Step 7: We define a gene by omics type combination as causal for SCZ if the causal effect test
822 passed the significance cutoff of FDR < 0.1 and the Egger intercept test passed the intercept p
823 value > 0.05 cutoff.

824 **One-sample Mendelian randomization**

825 For one-sample MR we used Two-stage predictor substitution (TSPS) approach, which is a
826 method to find causal relationships between omics types. We performed the following analysis in
827 two iterations, both following the direction of genetic information flow. In the first iteration, we
828 tested causal relationships between transcript level and ribosome occupancy level (i.e. mRNA ->
829 ribosome occupancy). In the second iteration, we tested causal relationships between ribosome
830 occupancy level and protein level (i.e. ribosome occupancy -> protein).

831 Step 1: We used LD clumping for instrument SNP selection as described in the previous section.
832 Here we tested two pathways (mRNA -> ribosome occupancy and ribosome occupancy ->
833 protein). For mRNA -> ribosome occupancy, we used the SNPs of eQTL with p value < 10^{-4} and
834 $R^2 < 0.5$ from LD. In order to test as many risk genes as we reasonably can, the same dynamic p
835 value cutoff approach (i.e. the same as the above described for two-sample MR) was used for

836 instrument SNP selection. See Supplemental Table 17 for details on the p value cutoffs used for
837 each risk gene.

838 Step 2: We then used the mr_steiger() function in the R package "TwoSampleMR" to test the
839 causal direction of selected instrument SNPs. For genes failing the Steiger test, we applied the
840 steiger_filtering() function to verify the direction of each instrument SNP and excluded those with
841 incorrect directions, ensuring the explained variance by the instrument SNPs was greater for the
842 exposure than for the outcome.

843 Step 3: We then combined genotype and quantification data of the relevant omics types into a
844 dataframe: dat_{mr} for mRNA -> ribosome occupancy pathway, dat_{rp} for ribosome occupancy ->
845 protein pathway.

846 Step 4: For each gene, we then set formula in R package "OneSampleMR" (*66*): tsps ("ribosome
847 occupancy ~ mRNA | SNP_1+SNP_2+SNP_3+…+SNP_n", data = dat_{mr}) and tsps ("protein ~ ribosome
848 occupancy | SNP_1+SNP_2+SNP_3+…+SNP_m", data = dat_{rp}).

849 Step 5: We used the summary() function to get the slope (i.e. the regression coefficient) and the
850 corresponding p value of the slope from each tsps object.

851 Step 6: We used Benjamini-Hochberg control procedure to adjust the p value of the slope for
852 multiple testing.

853 Step 7: We defined a relationship for each gene by pathway combination as causal if the test
854 results passed the significance cutoff of FDR < 0.1.

855 Step 8: We also used R package "ivreg" with the same dataset and formula as the above described
856 for tsps objects to calculate F-statistics for each gene. The calculated F-statistics was used to
857 check instrument strength.

858

859 **Data availability**

860 All raw data from psychENCODE BrainGVEX project are available through
861 https://www.synapse.org/#!Synapse:syn5613798.

862

863 **Code availability**

864 All code, and processed data used in the analyses are available at
865 https://github.com/qiumanL/multi-omics-qtl.

866

867 **References**

868 1. A. Fialkowski, T. M. Beasley, H. K. Tiwari, *Emery and Rimoin's Principles and Practice of*
869 *Medical Genetics and Genomics (Seventh Edition) Ch. 11*, (Academic Press, 2019).

870 2. A. S. Brown, The environment and susceptibility to schizophrenia. *Prog. Neurobiol*. **93**, 23–
871 58 (2011).

872 3. N. Solovieff, C. Cotsapas, P. H. Lee, S. M. Purcell, J. W. Smoller, Pleiotropy in complex
873 traits: challenges and strategies. *Nat. Rev. Genet.* **14**, 483–495 (2013).

874 4. K. Watanabe, E. Taskesen, A. van Bochoven, D. Posthuma, Functional mapping and
875 annotation of genetic associations with FUMA. *Nat. Commun.* **8**, 1826 (2017).

876 5. M. G. Heckman, et al., Fine-mapping of the non-coding variation driving the Caucasian
877 LRRK2 GWAS signal in Parkinson‘s disease. *Parkinsonism Relat. Disord*. **83**, 22–30
878 (2021).

879 6. D. J. Schaid, W. Chen, N. B. Larson, From genome-wide associations to candidate causal
880 variants by statistical fine-mapping. *Nat. Rev. Genet.* **19**, 491–504 (2018).

881 7. A. Gusev et al., Integrative approaches for large-scale transcriptome-wide association
882 studies. *Nat. Genet.* **48**, 245–252 (2016).

883 8. Wang, L. et al. Brain Banks Spur New Frontiers in Neuropsychiatric Research and
884 Strategies for Analysis and Validation. *Genomics Proteomics Bioinformatics.* **17**, 402–414
885 (2019).

886 9. ENCODE Project Consortium et al., Expanded encyclopaedias of DNA elements in the
887 human and mouse genomes. *Nature*. **583**, 699–710 (2020).

888 10. GTEx Consortium, The GTEx Consortium atlas of genetic regulatory effects across human
889 tissues. *Science*. **369**, 1318–1330 (2020).

890 11. C. Giambartolomei et al., Bayesian test for Colocalisation between pairs of genetic
891 association studies using summary statistics. *PloS Genet*. **10**, e1004383 (2014).

892 12. E. R. Gamazon et al., A gene-based association method for mapping traits using reference
893 transcriptome data. *Nat. Genet*. **47**, 1091–1098 (2015).

894 13. Z. Zhu et al., Integration of summary data from GWAS and eQTL studies predicts complex
895 trait gene targets. *Nat. Genet*. **48**, 481–487 (2016).

896 14. Bray, N. J. & O'Donovan, M. C. The genetics of neuropsychiatric disorders. *Brain Neurosci.*
897 *Adv*. **2**, 2398212818799271 (2018).

898 15. R. S. Kahn et al., Schizophrenia. *Nat. Rev. Dis. Primers*. **1**, 15067 (2015).

899 16. P. Lichtenstein et al., Common genetic determinants of schizophrenia and bipolar disorder in
900 Swedish families: a population-based study. *Lancet*. **373**, 234–239 (2009).

901 17. P. F. Sullivan, K. S. Kendler, M. C. Neale, Schizophrenia as a complex trait: evidence from
902 a meta-analysis of twin studies. *Arch Gen Psychiatry*. **60**, 1187–1192 (2003).

903 18. V. Trubetskoy et al., Mapping genomic loci implicates genes and synaptic biology in
904 schizophrenia. *Nature*. **604**, 502–508 (2022).

905 19. J. B. W. Wolf, Principles of transcriptome analysis and gene expression quantification: an
906 RNA-seq tutorial. *Mol Ecol Resour*. **13**, 559–572 (2013).

907 20. A. Battle, Z. Khan, S. H. Wang, A. Mitrano, M. J. Ford, J. K. Pritchard, Y. Gilad, Impact of
908 regulatory variation from RNA to protein. *Science*. **347**, 664–667 (2015).

909 21. E. Ferkingstad et al., Large-scale integration of the plasma proteome with genetics and
910 disease. *Nat. Genet*. **53**, 1712–1721 (2021).

911 22. Luo, J. et al. Genetic regulation of human brain proteome reveals proteins implicated in
912 psychiatric disorders. *Mol Psychiatry.* (2024).

913 23. C. Giambartolomei et al., A Bayesian framework for multiple trait colocalization from
914 summary association statistics. *Bioinformatics*. **34**, 2538–2545 (2018).

915 24. C. N. Foley et al., A fast and efficient colocalization algorithm for identifying shared genetic
916 risk factors across multiple traits. *Nat. Commun*. **12**, 764 (2021).

917 25. N. T. Ingolia, S. Ghaemmaghami, J. R. S. Newman, J. S. Weissman, Genome-wide analysis
918 in vivo of translation with nucleotide resolution using ribosome profiling. *Science*. **324**, 218–
919 223 (2009).

920 26. N. T. Ingolia, G. A. Brar, S. Rouskin, A. M. McGeachy, J. S. Weissman, The ribosome
921 profiling strategy for monitoring translation in vivo by deep sequencing of ribosome-
922 protected mRNA fragments. *Nat. Protoc*. **7**, 1534–1550 (2012).

923 27. Cenik C et al., Integrative analysis of RNA, translation, and protein levels reveals distinct
924 regulatory variation across humans. *Genome Res.* **25**, 1610-1621 (2015).

925 28. S. Akbarian et al., The PsychENCODE project. *Nat. Neurosci*. **18**, 1707–1712 (2015).

926 29. M. J. Gandal et al., Transcriptome-wide isoform-level dysregulation in ASD, schizophrenia,
927 and bipolar disorder. *Science*. **362**, eaat8127 (2018).

928 30. G. A. Brar, J. S. Weissman, Ribosome profiling reveals the what, when, where and how of
929 protein synthesis. *Nat. Rev. Mol. Cell Biol*. **16**, 651–664 (2015).

930 31. J. D. Storey, R. Tibshirani, Statistical significance for genomewide studies. *Proc. Natl.*
931 *Acad. Sci. U.S.A.* **100**, 9440–9445 (2003).

932 32. G. E. Hoffman et al., CommonMind Consortium provides transcriptomic and epigenomic
933 data for Schizophrenia and Bipolar Disorder. *Sci. Data*. **6**, 180 (2019).

934 33. Robins, C. et al. Genetic control of the human brain proteome. The American Journal of
935 Human Genetics 108, 400–410 (2021).

936 34. D. W. Yao, J. O'Connor, A. L. Price, A. Gusev, Quantifying genetic effects on disease
937 mediated by assayed gene expression levels. *Nat. Genet*. **52**, 626–633 (2020).

938 35. A. N. Barbeira et al., Exploring the phenotypic consequences of tissue specific gene
939 expression variation inferred from GWAS summary statistics. *Nat. Commun*. **9**, 1825
940 (2018).

941 36. S. Ripke et al., Biological insights from 108 schizophrenia-associated genetic loci. *Nature*.
942 **511**, 421–427 (2014).

943 37. A. F. Pardiñas et al., Common schizophrenia alleles are enriched in mutation-intolerant
944 genes and in regions under strong background selection. *Nat. Genet*. **50**, 381–389 (2018).

945 38. M. Lam et al., Comparative genetic architectures of schizophrenia in East Asian and
946 European populations. *Nat. Genet*. **51**, 1670–1678 (2019).

947 39. Gusev, A. et al. Transcriptome-wide association study of schizophrenia and chromatin
948 activity yields mechanistic disease insights. *Nat Genet.* **50**, 538–548 (2018).

949 40. Johnson RJ et al., Cerebral Fructose Metabolism as a Potential Mechanism Driving
950 Alzheimer's Disease. *Front Aging Neurosci*. **2**, 560865 (2020).

951 41. Sugatha, J. et al. Insights into cargo sorting by SNX32 and its role in neurite outgrowth.
952 *eLife*. **12**, e84396 (2023).

953 42. Korologou-Linden R, Leyden GM, Relton CL, Richmond RC, Richardson TG. Multi-omics
954 analyses of cognitive traits and psychiatric disorders highlights brain-dependent
955 mechanisms. *Hum Mol Genet.* **32**, 885–96 (2021).

956 43. D. Zhou, Y. Jiang, X. Zhong, N. J. Cox, C. Liu, E. R. Gamazon, A unified framework for
957 joint-tissue transcriptome-wide association and Mendelian randomization analysis. *Nat.*
958 *Genet*. **52**, 1239–1246 (2020).

959 44. S. Burgess, S. G. Thompson, Interpreting findings from Mendelian randomization using the
960 MR-Egger method. *Eur. J. Epidemiol*. **32**, 377–389 (2017).

961 45. S. Purcell et al., PLINK: A Tool Set for Whole-Genome Association and Population-Based
962 Linkage Analyses. *Am. J. Hum. Genet.* **81**, 559–575 (2007).

963 46. A. Gkatzionis, S. Burgess, P. J. Newcombe, Statistical methods for cis-Mendelian
964 randomization with two-sample summary-level data. *Genet. Epidemiol*. **47**, 3–25 (2023).

965 47. Burgess, S., Dudbridge, F., Thompson, S. G. Combining information on multiple
966 instrumental variables in Mendelian randomization: comparison of allele score and
967 summarized data methods. *Statist. Med.* **35**, 1880–1906 (2016).

968 48. Zou Y, Carbonetto P, Wang G, Stephens M. Fine-mapping from summary data with the
969 "Sum of Single Effects" model. *PloS Genet*. **18**, e1010299 (2022).

970 49. C. G. Artieri, H. B. Fraser, Evolution at two levels of gene expression in yeast. *Genome Res.*
971 **24** (2014).

972 50. C. J. McManus, G. E. May, P. Spealman, A. Shteyman, Ribosome profiling reveals post-
973 transcriptional buffering of divergent gene expression in yeast. *Genome Res*. **24**, 422–430
974 (2014).

975 51. F. W. Albert, D. Muzzey, J. S. Weissman, L. Kruglyak, Genetic influences on translation in
976 yeast. *PloS Genet*. **10**, e1004692 (2014).

977 52. Niu M, Cho JH, Kodali K, Pagala V, High AA, Wang H et al. Extensive peptide
978 fractionation and y 1 ion-based interference detection method for enabling accurate
979 quantification by isobaric labeling and mass spectrometry. *Anal Chem*. **89**(5), 2956-2963
980 (2017).

981 53. Mullins, N. et al. Genome-wide association study of more than 40,000 bipolar disorder cases
982 provides new insights into the underlying biology. *Nat Genet*. **53**, 817–829 (2021).

983 54. Autism Spectrum Disorders Working Group of The Psychiatric Genomics Consortium.
984 Meta-analysis of GWAS of over 16,000 individuals with autism spectrum disorder

985 highlights a novel locus at 10q24.32 and a significant overlap with schizophrenia. *Mol*
986 *Autism* **8**, 21 (2017).

987 55. Meng, X. *et al.* Multi-ancestry genome-wide association study of major depression aids
988 locus discovery, fine mapping, gene prioritization and causal inference. *Nat Genet* **56**, 222–
989 233 (2024).

990 56. B. Li, C. N. Dewey, RSEM: accurate transcript quantification from RNA-Seq data with or
991 without a reference genome. *BMC Bioinformatics*. **12**, 323 (2011).

992 57. M. C. Oldham, P. Langfelder, S. Horvath, Network methods for describing sample
993 relationships in genomic datasets: application to Huntington‘s disease. *BMC Syst. Biol.* **6**, 63
994 (2012).

995 58. B. M. Bolstad, R. A. Irizarry, M. Astrand, T. P. Speed, A comparison of normalization
996 methods for high density oligonucleotide array data based on variance and bias.
997 *Bioinformatics*. **19**, 185–193 (2003).

998 59. Y. Jiang et al., DRAMS: A tool to detect and re-align mixed-up samples for integrative
999 studies of multi-omics data. *PloS Comput. Biol.* **16**, e1007522 (2020).

1000 60. B. Langmead, S. L. Salzberg, Fast gapped-read alignment with Bowtie 2. *Nat. Methods*. **9**,
1001 357–359 (2012).

1002 61. Y. Liao, G. K. Smyth, W. Shi, featureCounts: an efficient general purpose program for
1003 assigning sequence reads to genomic features. *Bioinformatics*. **30**, 923–930 (2014).

1004 62. O. Stegle, L. Parts, M. Piipari, J. Winn, R. Durbin, Using probabilistic estimation of
1005 expression residuals (PEER) to obtain increased power and interpretability of gene
1006 expression analyses. *Nat. Protoc*. **7**, 500–507 (2012).

1007 63. O. Delaneau, H. Ongen, A. A. Brown, A. Fort, N. I. Panousis, E. T. Dermitzakis, A
1008 complete tool set for molecular QTL discovery and analysis. *Nat. Commun*. **8**, 15452 (2017).

1009 64. B. L. Pierce, S. Burgess, Efficient Design for Mendelian Randomization Studies: Subsample
1010 and 2-Sample Instrumental Variable Estimators. *Am. J. Epidemiol.* **178**, 1177–1184 (2013).

1011 65. Yavorska O, Burgess S. MendelianRandomization: an R package for performing Mendelian
1012 randomization analyses using summarized data. *Int J Epidemiol*. **46**(6) (2017).

1013 66. Terza, J. V., Basu, A. Rathouz, P. J. Two-stage residual inclusion estimation: Addressing
1014 endogeneity in health econometric modeling. *Journal of Health Economics.* **27**, 531–543
1015 (2008).

1016

1017 **Acknowledgments**

1018 We thank the three anonymous reviewers for their valuable comments, which resulted in
1019 substantial improvement of the manuscript. We thank Majd Alsayed, Miguel Brown, Dominic
1020 Fitzgerald, Amber Thomas, and Mimi Brown for their assistance with RNA-Seq data production
1021 and processing. We thank Richard Kopp at SUNY Upstate Medical University for his help with
1022 wordsmithing. We thank all of the donors and their relatives participated in the brain collections
1023 at Stanley Medical Research Institute and Banner Sun Health Research Institute. We thank Drs.
1024 Maree J. Webster and Thomas Beach for their supports to make the tissue available. We thank the

1025 High Performance Computing Center of Central South University for partial support of
1026 calculation. This project has received funding from National Key Research and Development
1027 Program of China (2024YFA1108000), National Natural Science Foundation of China (Grants
1028 No. 82022024), SUNY Empire Innovation Program, National Institutes of Health grants
1029 (U01MH122591, U01MH116489, R01MH110920, R01MH126459, U01MH103340,
1030 R01MH109715, R01MH110555, R21MH129817, R01GM139980).

1031 **Author contributions**

1032 CL, KPW, JP, SHW, BL, XW, CC were responsible for Conceptualization. AWS, LC, DZ, FW,
1033 MX, MN, DP, YJW, RV, CZ, KG, GG were responsible for sample collection, DNA extraction,
1034 mRNA extraction, mRNA binding with ribosome extraction, protein extraction, sequencing, mass
1035 spectrum and raw data processing. SHW, QL, YJ, CC, CY, AWS were responsible for
1036 investigation of analysis. QL was responsible for visualization of results. SHW, CL, CC, BL,
1037 KPW were responsible for supervision. SHW, QL, YJ, CL were responsible for original draft
1038 writing. SHW, CL, CC, QL were responsible for review and editing.

1039

1040 **Competing interests**

1041 Authors declare that they have no competing interests.

1042

1043 **Figures and Tables**

1044

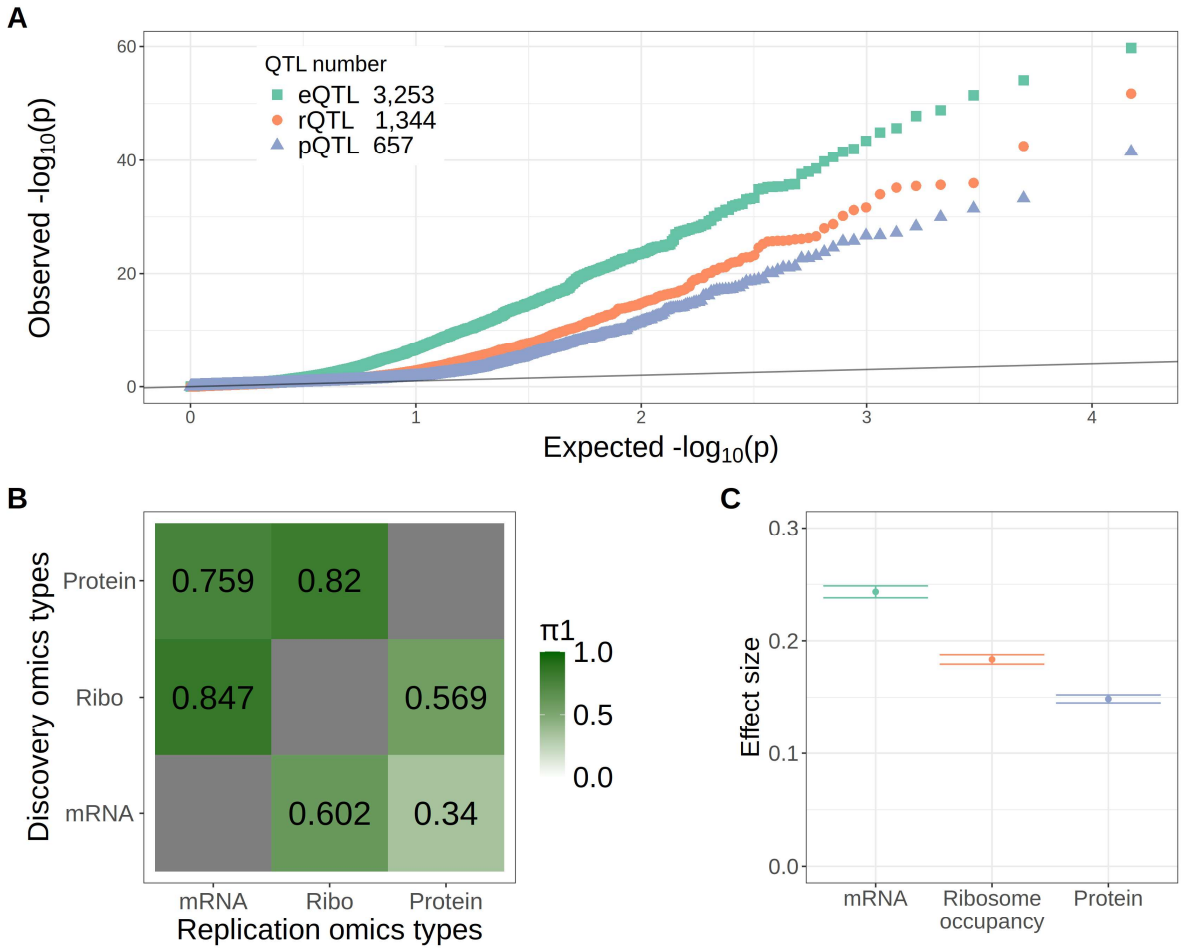

1045

1046 **Fig. 1. Genetic regulation of gene expression in the human brain. (A)** P-value quantile-
1047 quantile plot between the observed (Y-axis) and the expected based on null distribution (X-axis).
1048 The black line indicates the expected distribution of p values when there are no real QTL signals.
1049 The number of cis-QTLs (i.e. the most significantly associated SNP for each gene) identified at
1050 10% FDR is labeled in the top left inset. **(B)** Replication rate between QTL types. Proportions of
1051 QTLs replicated in the other two omics types are listed in the 3 × 3 matrix. Each row is a
1052 discovery omics type and each element of the row correspond to the proportion QTL signals

1053 replicated in the omics type specified by the column label. For example, only 34% of the eQTL
1054 signals were replicated in the protein data. Ribo: ribosome occupancy. **(C)** Effect size of CMC
1055 eQTL SNPs in BrainGVEX data. Mean and 95% confidence interval of absolute per allele effect
1056 across all CMC eQTL SNPs that were also analyzed in the BrainGVEX union set is shown.

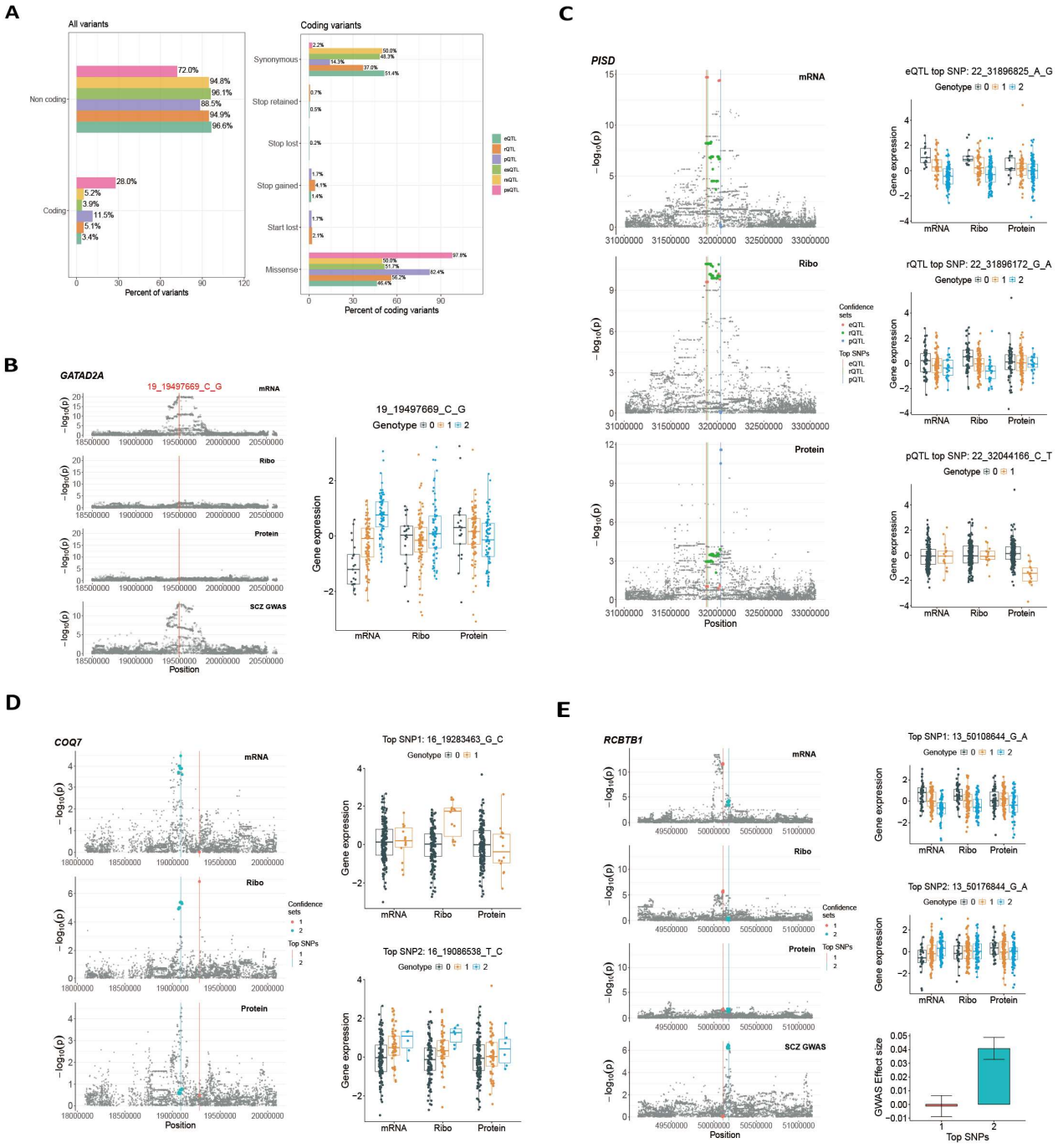

Fig. 2. Omics-specific genetic regulations. (**A**) Categorizing QTL SNPs according to genic feature annotations. Bar plots showing the percentage of QTL SNPs in each category out of the total number of QTL SNPs considered. Note the high percentage (28%) of coding variants in psQTL SNPs out of all psQTL SNPs and the dominating percentage (97.8%) of missense variants in psQTL SNPs out of coding psQTL SNPs. (**B**) An example SCZ risk gene, *GATAD2A,* with

predominantly transcript specific QTL effects. The red line indicates the top signal colocalization SNP between eQTL and SCZ GWAS on a Manhattan plot. Boxplots to the right summarize the normalized gene expression level stratified by eQTL SNP genotypes. Ribo: ribosome occupancy. (**C, D, E**) Example genes containing multiple QTL signals of varying omics specificity. Individual confidence set SNPs containing 95% of the QTL signal are color coded on a Manhattan plot with a vertical line indicating the top SNP that contributes the most signal. Boxplots to the right summarize the normalized gene expression level stratified by genotypes of the top SNP. Note that the example gene in (E) is a SCZ risk gene with two confidence sets. Only one of the two confidence sets' QTL signal colocalizes with SCZ GWAS signal. The bar plots underneath the expression level boxplots show the log odds ratio +/- standard errors for the association between the confidence set top SNP genotype and SCZ, which is calculated based on GWAS summary statistics from Trubetskoy et al.

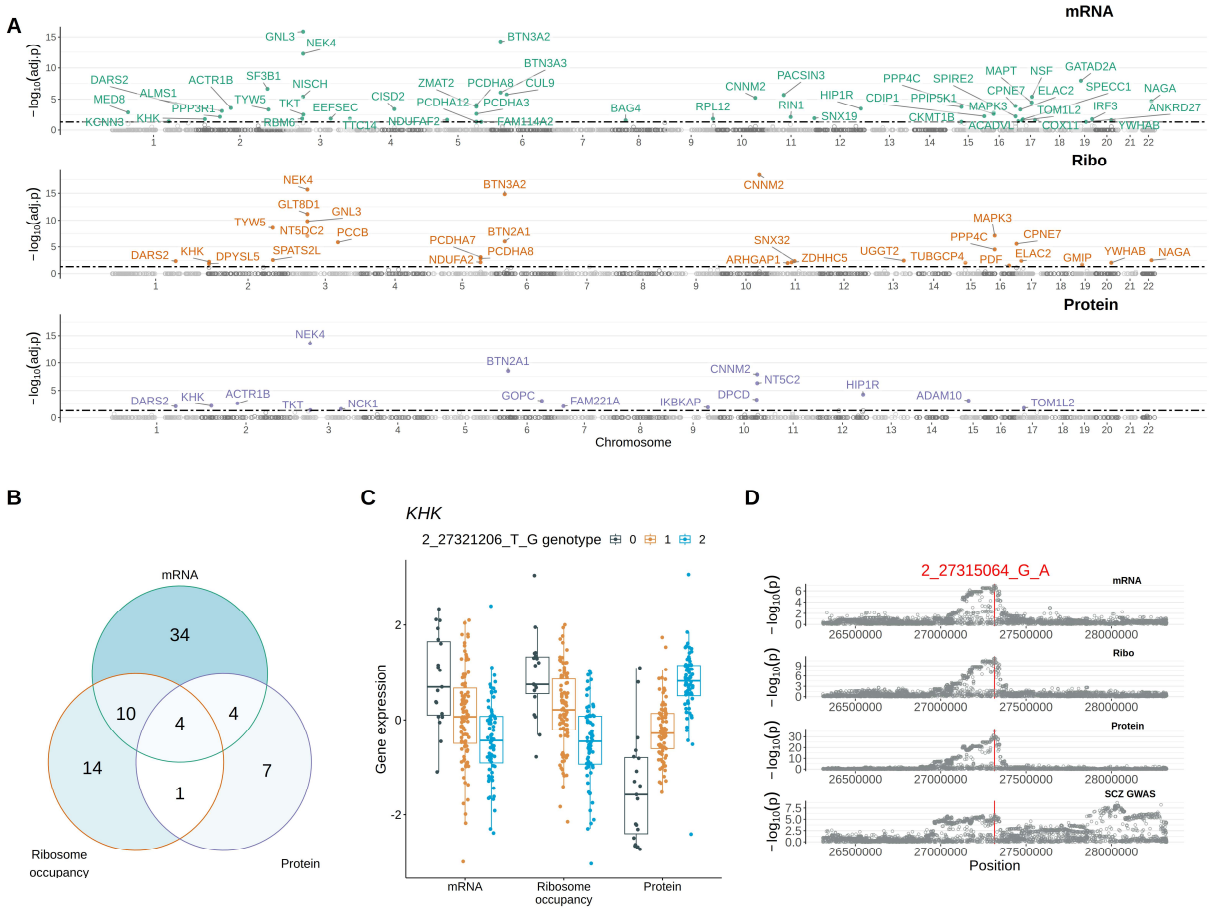

Fig. 3. Schizophrenia risk genes identified from each of the three omics types, RNA-Seq (mRNA), ribo-seq (ribosome occupancy), and quantitative mass spectrometry (protein), using S-PrediXcan. (A) Manhattan plots showing significance level (i.e. -log10 FWER from S-PrediXcan) of gene expression-schizophrenia association across the genome for genes that pass the 5% FWER significance cutoff for each omics type. The black horizontal dotted line indicated the significance cutoff (5% Bonferroni-adjusted p value). Ribo: ribosome occupancy. **(B)** Venn diagram illustrating the number of overlapping risk genes identified between omics types. **(C)** Boxplots summarizing normalized gene expression level stratified by eQTL SNP genotypes for *KHK*. **(D)** Manhattan plots showing nominal p value distribution for each QTL type and

1091 schizophrenia GWAS for the 1Mb QTL mapping window flanking *KHK*. The red line indicates

1092 the position of the lead colocalization SNP between eQTLs and schizophrenia GWAS.

1093

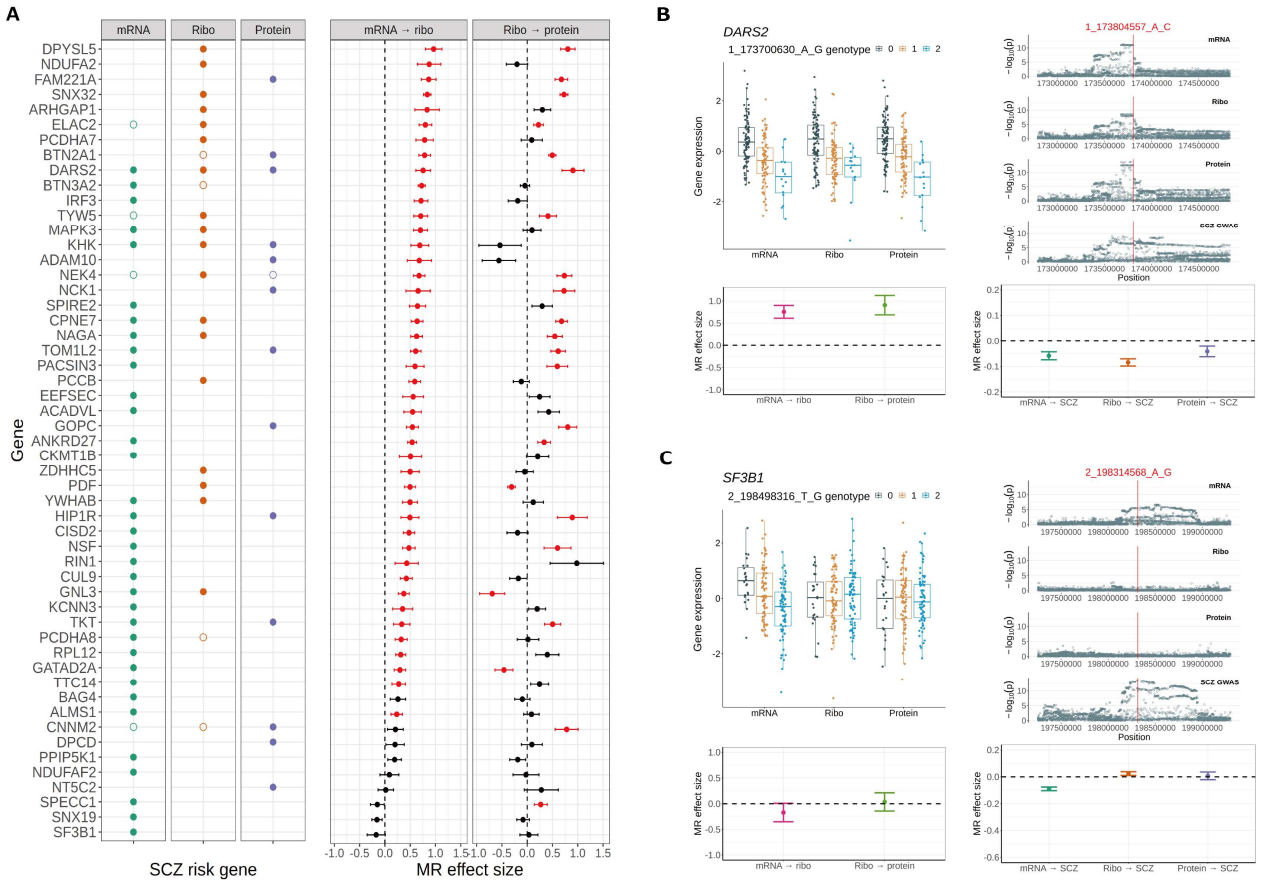

Fig. 4. Identifying driver regulatory mechanism for SCZ risk genes using Mendelian Randomization (MR). (A) Summaries of MR test results. Left panel: Two-sample MR replication of S-PrediXcan SCZ risk gene discoveries. Each circle represents a S-PrediXcan discovery. A solid-colored circle indicates successful replication in a MR test. Right panel: One-sample MR test results for causality between omics types. Shown are MR effect size +/- the corresponding standard errors. Red data points indicate significant test results. Ribo: ribosome occupancy. (**B, C**) Example SCZ risk genes driven by either transcriptional regulation of protein expression (B) or transcript specific effects (C). Boxplots on the left summarize the normalized gene expression level stratified by QTL SNP genotypes. The effect size estimates from the corresponding one-sample MR causality test between each pair of omics are shown in the plot

1107 beneath. Manhattan plots on the right show nominal p values for all variants in the QTL mapping
1108 window for each omics and SCZ GWAS with the red vertical line indicating the top signal
1109 colocalization SNP between QTLs and GWAS. Directly underneath the Manhattan plots are
1110 effect size estimates from the corresponding two-sample MR tests replicating the risk gene
1111 discoveries.